

# DFT BASED MIMO-OFDM Channel Estimation for Orthogonal Time Frequency Space (OTFS)

CH. Rajesh babu<sup>1</sup>; CH. Asha<sup>2</sup>; B. Ramana<sup>3</sup>; S. Manikanta<sup>4</sup>; CH. Phani kumar<sup>5</sup>

<sup>1</sup>Assistant Professor, Department of Electronics and Communication Engineering, Godavari Institute of Engineering and Technology(autonomous),Rajahmundry, Andhra Pradesh, India

<sup>2,3,4,5</sup>UG Student, Department of Electronics and Communication Engineering, Godavari Institute of Engineering and Technology(autonomous),Rajahmundry, Andhra Pradesh, India

**Abstract:** In high-mobility situations, orthogonal time frequency space (OTFS) modulation outperforms orthogonal frequency division multiplexing (OFDM). Due to the large pilot overhead needed for OTFS massive MIMO, downlink channel estimate is a problem. In this article, we present a channel estimation method based on the 3D structured orthogonal matching pursuit (3D-SOMP) algorithm. First, we demonstrate that the OTFS MIMO channel has three types of sparsity: normal sparsity in the delay dimension, block sparsity in the Doppler dimension, and burst sparsity in the angle dimension. We next construct the downlink channel estimation issue as a sparse signal recovery problem based on the 3D structured channel sparsity. The proposed 3D-SOMP method achieves accurate channel state information with minimal pilot overhead, according to simulation findings.



Check for updates



\* DOI of the Article: <https://doi.org/10.46501/IJMTST0707009>

Available online at: <http://www.ijmtst.com/vol7issue07.html>



As per **UCC guidelines** an electronic bar code is provided to secure your paper

To Cite this Article:

CH. Rajesh babu; CH. Asha; B. Ramana; S. Manikanta; CH. Phani kumar. DFT BASED MIMO-OFDM Channel Estimation for Orthogonal Time Frequency Space (OTFS). *International Journal for Modern Trends in Science and Technology* 2021, 7, 0707030, pp. 50-56. <https://doi.org/10.46501/IJMTST0707009>

Article Info.

Received: 14 May 2021; Accepted: 2 July 2021; Published: 10 July 2021

## I. INTRODUCTION

One aim of future wireless communications (the coming 5G or beyond 5G) is to enable reliable communications in high-mobility situations, such as on high-speed trains capable of reaching 500 km/h [1] or automobiles capable of reaching 300 km/h [2]. Orthogonal frequency division multiplexing is the most used modulation method for 4G and future 5G networks (OFDM). Because of the wide Doppler spread of time-variant channels, OFDM may suffer substantial inter-carrier interference (ICI) in high-mobility situations. When conventional transceivers are utilised, ICI will significantly impair the performance of OFDM systems. Some adaptations of the conventional OFDM have been suggested to deal with ICI at the expense of more complex transceiver design [3]–[7].

Orthogonal time frequency space (OTFS) is a time-variant channel alternative to OFDM [8]–[10]. OTFS transforms time-variant channels into time-independent channels in the delay-Doppler domain using the basis expansion model for the channel [11]. As a result, the information-carrying data is multiplexed into the delay-Doppler domain's approximately constant channels. Massive multiple-input multiple-output (MIMO) OTFS may improve spectrum efficiency even further. Such advantages need knowing the downlink channel status information (CSI) at the transmitter.

To create the vectors for transmit beam forming [12]. Downlink channel estimate in OTFS huge MIMO systems with a large number of base station (BS) antennas is difficult owing to the high pilot overhead needed.

For channel estimate in OTFS systems, the BS employs pilots that are broadcast in the delay-Doppler domain [13]. An impulse-based approach for single-input single-output (SISO) systems was suggested, in which training pilots were broadcast as a delay-Doppler impulse. It was extended to OTFS MIMO systems by sending several impulses with appropriate guard between neighbouring impulses to differentiate between distinct BS antennas [14]. In [15], an alternate technique for OTFS SISO channel estimation was suggested, which used PN sequences in the delay-Doppler domain as training pilots. Three channel coefficients, namely delay shift, Doppler shift, and fade

coefficient, are calculated using this technique. The delay-Doppler channel may then be computed as needed. Because a large number of antennas must be differentiated by broadcasting orthogonal pilots, current OTFS channel estimation methods cannot be easily applied to OTFS massive MIMO systems, resulting in significant pilot overhead.

In this work, we present a downlink channel estimate method for OTFS large MIMO systems based on 3D structured orthogonal matching pursuit (3D-SOMP) algorithm. We describe the discrete-time formulation of OTFS systems and demonstrate that the OTFS massive MIMO channel has a delay-Doppler-angle 3D structured sparsity, thanks to the channel estimator's usage of delay-Doppler-domain training pilots. We frame the channel estimation issue as a sparse signal recovery problem by decomposing the channel based on its structure. We present a 3D-SOMP method to address this issue, which can obtain accurate CSI with minimal pilot overhead.

## II. SYSTEM MODEL

The discrete-time formulation of OTFS modulation and OTFS demodulation in SISO systems is presented in this section. Then we explain how OTFS may be extended to large MIMO systems.

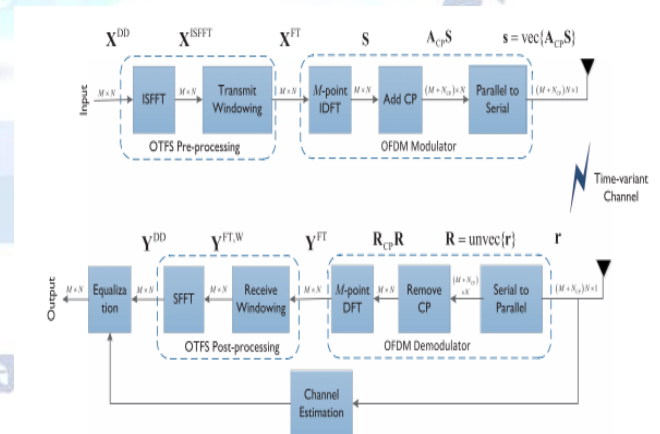


**Fig. 1.** OTFS SISO architecture. OTFS modulation is composed of a pre-processing block before a traditional OFDM modulator at the transmitter. OTFS demodulation is composed of a post-processing block after a traditional OFDM demodulator at the receiver.

### A. SISO Modulation in OTFS

The OTFS SISO architecture is taken as widely accepted [8]–[10]. First, an  $MN$ -length quadrature amplitude modulated (QAM) data stream is reorganised into a 2D

data block. This is referred to as a 2D OTFS  $X^{DD} \in \mathbb{C}^{M \times N}$  M and N are the numbers of resource units along the delay and Doppler dimensions, respectively, in the delay-Doppler domain. A pre-processing block and a conventional frequency-time modulator, such as OFDM or filter bank multicarrier, are used in OTFS modulation at the transmitter (FBMC). An inverse simplistic finite Fourier transform (ISFFT) and a transmit windowing function are used to implement the pre-processing step. The ISFFT of  $X^{DD}$  is [8]

$$X^{ISFFT} = F_M X^{DD} F_N^H \quad (1)$$

A transmit windowing matrix  $W^{tx} \in \mathbb{C}^{M \times N}$  multiplies  $X^{ISFFT}$  element-wise to produce the 2D block in the frequency-time domain  $X^{FT} \in \mathbb{C}^{M \times N}$

$$X^{FT} = X^{ISFFT} \oslash W^{tx} \quad (2)$$

The windowing matrix may be used for a variety of purposes, including randomising the phases of transmitted signals to minimise inter-cell interference [13]. In this article, we assume that simple expressions have a trivial window, i.e.  $W^{tx}$  is a matrix of all ones.

On each column, the M-point inverse DFT (IDFT) is implemented, assuming an OFDM modulator. The 2D transmit signal block is

$$S = F_M^H X^{FT} \quad (3)$$

Where  $S = [s_1, s_2, \dots, s_N]$  Each column vector  $s_i \in \mathbb{C}^{M \times 1}$  can be regarded as an OFDM symbol By combing (1)-(3),

$$S = X^{DD} F_N^H \quad (4)$$

The OFDM modulator typically inserts a cyclic prefix (CP) for each OFDM signal to prevent inter-symbol interference between blocks. the 1D transmit signal  $s_i \in \mathbb{C}^{(M+N_{CP}) \times 1}$  is

$$s = \text{vec}\{A_{CP} S\} \quad (5)$$

**B. Demodulation of the OTFS SISO**

At the receiver, the  $k^{\text{th}}$  element  $r_k$  of the received signal

$$r_k = \sum_{l=0}^L h_{k,l} s_{k-l} + v_k \quad (6)$$

Where  $s_{k-l}$  is the  $(k-l)^{\text{th}}$  element of the transmit signal  $s$  and  $v_k$  is the additive Gaussian noise at the receiver.

A conventional frequency-time demodulator, such as the OFDM or FBMC demodulator, plus a post-processing block make up the OTFS demodulation at the receiver. In the case of an OFDM demodulator, the received signal  $r$  is reorganised first as a matrix  $R$  of size  $(M + N_{CP}) \times N$

**C. Massive MIMO OTFS**

We show how OTFS works in large MIMO systems to improve spectrum efficiency even further by using multi-user MIMO. The BS has  $N_t$  antennas to serve  $U$  single-antenna customers at the same time. To minimise inter-user interference, downlink precoding is used. The zero-forcing Tomlinson-Harashimaprecoding, for example, is used in [12]. The transmit data block  $X^{DD}$  in the delay-Doppler domain will be modulated using the OTFS modulation and sent at  $N_t$  antennas after precoding. The received signal is demodulated at the user's end using the OTFS demodulation. Due to the necessary high pilot overhead, the primary difficulty with OTFS large MIMO is downstream channel estimate. Next, we'll look into large MIMO systems' downlink channel estimate.

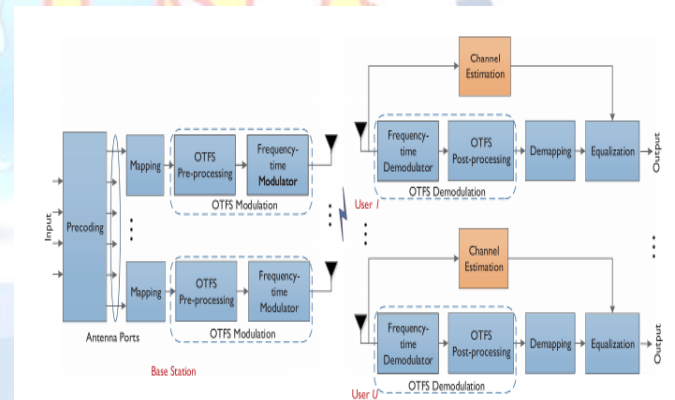


**Fig. 2.** OTFS massive MIMO architecture. Multi-user MIMO is used to increase the spectrum efficiency. Downlink precoding is performed based on the downlink CSI [28], which is obtained through downlink channel estimation and uplink channel feedback in FDD systems.

**III. PROPOSED 3D-SOMP BASED CHANNEL ESTIMATION IN OTFS MASSIVE MIMO SYSTEMS**

The 3D structured sparsity of OTFS MIMO channels is first shown in this section. The downlink channel estimation issue is then reformulated as a sparse signal recovery problem, which is solved using the 3D-SOMP method.



### A. Delay-Doppler-angle Channel Sparsity in 3D Structure

We examine a time-variant downlink channel with  $N_p$  dominating propagation routes. There are  $N_s$  sub paths in each dominating path. The  $i$ -th dominant path's  $s_i$ -th sub path has a complicated path gain of  $\alpha_{s_i}$  and a Doppler frequency of  $\nu_{s_i}$ . The time-variant channel associated with the  $(p+1)^{th}$  antenna ( $p = 0, 1, 2, \dots, N_t - 1$ ) can be expressed as [18]

$$h_{k,l,p} = \sum_{i=1}^{N_p} \sum_{s_i=1}^{N_s} \alpha_{s_i} e^{j2\pi\nu_{s_i}kT_s} \text{Pr}c\left(lT_s - \tau\right) e^{j2\pi\nu_{s_i}lT_s} \quad (7)$$

Where  $\text{pr}c(\tau)$  is the band-limited pulse shaping filter response

The delay-Doppler-angle channel  $H_{l,k,r}^{DDA}$  is defined by

$$H_{l,k,r}^{DDA} = \text{IDFT} \left\{ H_{l,k,r}^{DDS} \right\} \text{ along the space-dimension } p$$

$$H_{l,k,r}^{DDA} = \sum_{p=0}^{N_t-1} H_{l,k,r}^{DDS} e^{j2\pi\frac{rp}{N_t}} \quad (8)$$

To summarise, the 3D channel tensor  $H$  is sparse along the delay axis, block sparse along the Doppler axis, and burst sparse along the angle axis. With minimal pilot overhead, this 3D structured sparsity may be utilised to predict the CSI.

### B. Downlink Channel Estimation Formulation

The length of pilots along the Doppler dimension and the delay dimension are denoted by the letters  $N_v$  and  $M\tau$ , respectively. As training pilots, we suggest using complicated Gaussian random sequences. Guard intervals are needed to prevent interference between pilots and data produced by 2D periodic convolution in the delay-Doppler domain. We propose the non-orthogonal pilot pattern to minimise total pilot overhead in OTFS huge MIMO systems, in which the pilots broadcast at separate antennas fully overlap in the delay-Doppler domain, while the training sequences at different antennas are produced independently.

$$y_{l,k} = \sum_{p=0}^{N_t-1} \sum_{l'=0}^{M_g-1} \sum_{k'=-\frac{N_g}{2}}^{\frac{N_g}{2}-1} w_{l-l',k-k'} H_{l',k'}^{DDS} p^{x_i-l',k-k',p} + v_{l,k} \quad (9)$$

We arrange  $y_{l,k}$  and  $H_{l,k,r}^{DDA}$  into column vectors

$$y = \sum_{r=-\frac{N_t}{2}}^{\frac{N_t}{2}-1} W \square Z_{c,r} h_r + v \quad (10)$$

## IV. SIMULATION RESULTS

The performance of the suggested 3D-SOMP based channel estimation method in terms of the normalised mean square error (NMSE) of channel estimation is investigated in this section. The conventional channel estimate method is based on impulses.

As a benchmark, a method that has been extended to MIMO systems is given [14]. For contrast, we show the NMSE of a conventional OMP-based channel estimating method, in which the OMP algorithm is employed to recover  $h$  in the channel. We use 3GPP to simulate a standardised spatial channel model in an urban macro cell setting [17]. Table I summarises the full system parameters. The pilot overhead ratio is defined as the ratio of the number of resource units used for pilot transmission to the total number of resource units used in the delay-Doppler domain

TABLE I

SYSTEM PARAMETERS FOR SIMULATION

Parameter	Values
Carrier frequency (GHz)	2.15
Duplex mode	FDD
Subcarrier spacing (kHz)	15
Cyclic prefix duration (us)	16.6
FFT size	1024
Transmission bandwidth (# of resource blocks)	50
Size of a OTFS frame (M, N)	(600, 12)
# of BS antennas	8 ~ 64
# of user antennas	1
Channel model: 3GPP standardized channel model	Urban macro cell
# of dominant channel paths	6
# of sub-paths per dominant path	20
User velocity (km/h)	360

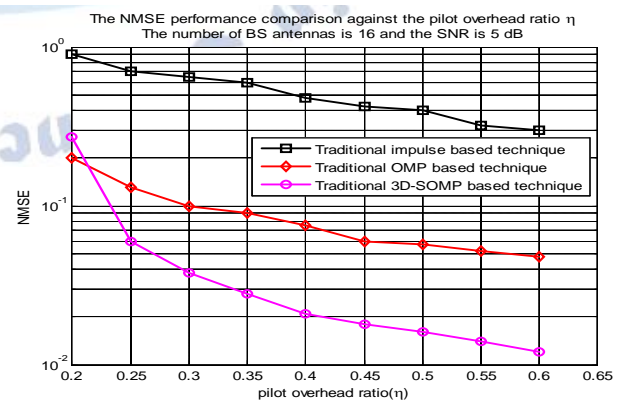


Fig. 3. The NMSE performance comparison against the pilot overhead ratio  $\eta$ . The number of BS antennas is 16 and the SNR is 5 dB.

The performance of the NMSE is compared to the pilot overhead ratio in Fig. 5. The user velocity is 100 m/s,

and there are 16 BS antennae. The SNR is 5 dB. When the same pilot overhead ratio is used, the suggested 3D-SOMP based channel estimation method outperforms the conventional impulse based channel estimation technique. Considered. The conventional impulse-based method does not work. Due to a lack of pilot overhead, the pilot performs effectively. The overhead ratio is low, i.e. the distance between two neighbouring points is short. Along the Doppler dimension and impulses are less than  $N_{max}$ . Along the delay dimension, and/or smaller than  $M_{max}$ . Therefore, The NMSE performance of the conventional impulse-based channel estimate will be harmed by interference from neighbouring impulses.

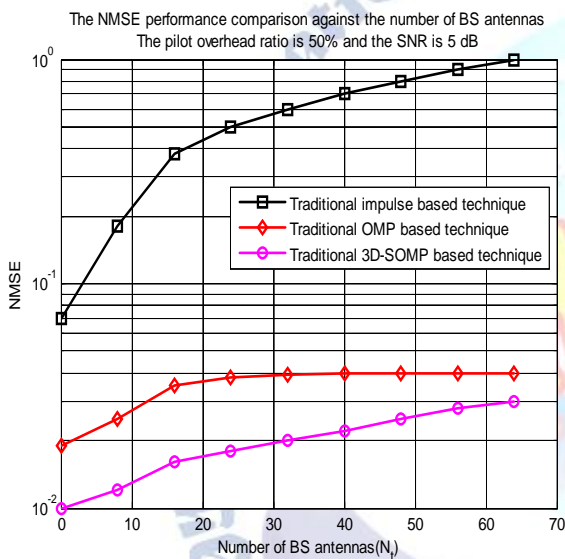


Fig. 4. The NMSE performance comparison against the number of BS antennas. The pilot overhead ratio is 50% and the SNR is 5 dB.

The NMSE performance is shown against the number of BS antennas  $N_t$  in Fig. 4. The pilot overhead ratio is set to 50%, the SNR is set to 5 decibels, and the user velocity is set to 100 metres per second. We see that the NMSE traditional performance is very good. When the number of BS antennas reaches 8, the impulse based channel estimation method declines significantly (NMSE is more than 101). When the number of BS antennas is high and the pilot overhead ratio is constant, this is due to inadequate gaps between two adjacent impulses. The suggested 3D-SOMP-based channel estimation method, on the other hand, performs well with a high number of BS antennas. As  $N_t$  grows, the performance difference between the proposed 3D-SOMP method and the

conventional OMP algorithm narrows. Because the 3D-SOMP method makes advantage of the structural sparsity of the 3D channel, it suffers from performance deterioration when there are insufficient pilots. The pilot overhead or SNR may be increased to address this issue.

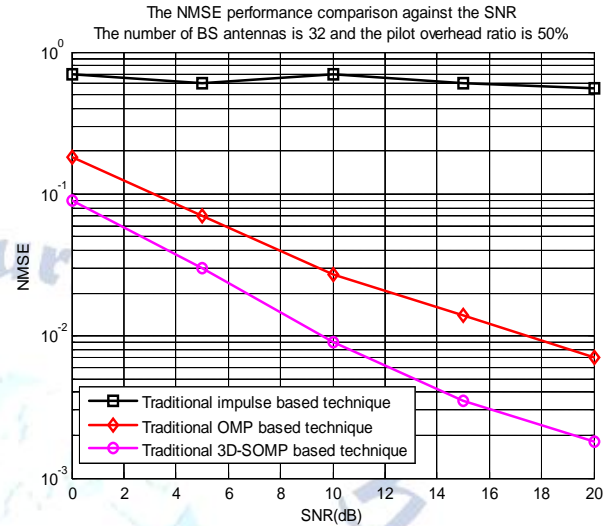


Fig. 5. The NMSE performance comparison against the SNR. The number of BS antennas is 32 and the pilot overhead ratio is 50%.

The performance of the NMSE versus the SNR is shown in Fig. 5. The user velocity is set to 100 m/s, the pilot overhead ratio is set to 50%, and the number of antennae is set to 32. The suggested 3D-SOMP-based channel estimation method outperforms the conventional impulse-based channel estimation technique, according to our findings. Due to interference among many antennas caused by inadequate bandwidth, the conventional impulse-based channel estimate method has an NMSE floor.

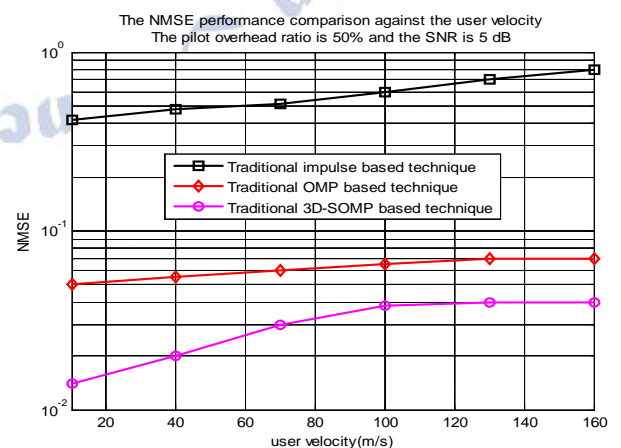
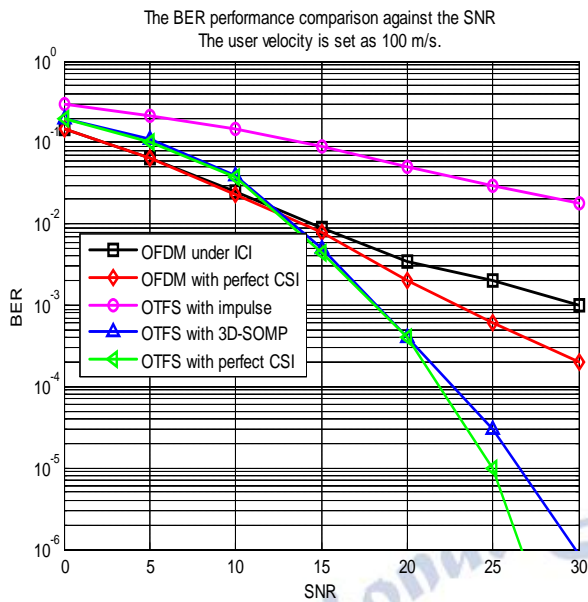


Fig. 6. The NMSE performance comparison against the user velocity. The pilot overhead ratio is 50% and the SNR is 5 dB.



**Fig. 7.** The BER performance comparison against the SNR. The user velocity is set as 100 m/s.

a pilot in the sky The NMSE performance of the proposed 3D-SOMP-based method improves with increasing SNR. Furthermore, by approximately 6 dB, the suggested 3D-SOMP-based method surpasses the conventional OMP-based technique.

In Figure 6, we compare the NMSE performance to the user velocity  $v$ . The pilot overhead ratio is  $\eta=50\%$ , and the SNR is 5 decibels. As the user velocity rises, the NMSE performance of channel estimation decreases. As a result, the necessary pilot overhead is raised in order to maintain a consistent NMSE. In our simulation, the NMSE performance of channel estimation decreases as the user velocity rises with a constant pilot overhead of  $\eta=50\%$ .

Finally, in Fig. 7, we compare the bit-error-rate (BER) to the signal-to-noise ratio (SNR) for both OFDM and OTFS systems. The user's speed is 100m/s. The ICI produced by the huge Doppler spread affects the BER performance of OFDM systems in this high-mobility scenario, as demonstrated by the curve "OFDM under ICI." With complete CSI information, we utilise MMSE detection to overcome ICI, as demonstrated by the curve "OFDM with perfect CSI," which beats "OFDM with ICI." Perfect CSI, estimated CSI using the conventional impulse-based approach, and estimated CSI using our new 3D-SOMP algorithm are all utilised in the OTFS system for OTFS signal identification through delayDoppler 2D deconvolution. In the presence of complete CSI information, the OTFS system outperforms the OFDM system in the high SNR

domain. This is due to the fact that transmit data in OTFS systems may take use of complete frequency-time channel diversity. We also found that the suggested 3D-SOMP method can provide satisfactory BER performance, which is quite similar to that of OTFS systems with perfect CSI. The conventional impulse-based channel estimate technique yields incorrect CSI, resulting in lower BER.

## VI. CONCLUSIONS

For the first time, we looked into OTFS modulation for large MIMO systems with an emphasis on channel estimation in this work. In OTFS huge MIMO systems, we specifically converted time-variant massive MIMO channels into delay-Doppler-angle 3D channels. The 3D channel is sparsely organised, i.e. sparse along the latency dimension, blocksparse along the Doppler dimension, and burst-sparse along the angle dimension, according to our findings. We framed the downlink channel estimation issue as a sparse signal recovery problem and addressed it using the suggested 3D-SOMP method based on 3D structured sparsity. The improved performance of our suggested method was confirmed by simulation results. In the future, we'll concentrate on a few outstanding issues in OTFS large MIMO systems, such as the low-complexity equaliser, downlink precoding, and efficient channel feedback.

## REFERENCES

1. B. Ai, X. Cheng, T. Krner, Z. D. Zhong, K. Guan, R. S. He, L. Xiong, D. W. Matolak, D. G. Michelson, and C. Briso-Rodriguez, "Challengestoward wireless communications for high-speed railway," *IEEE Trans.Intell. Transport. Syst.*, vol. 15, no. 5, pp. 2143–2158, Oct. 2014.
2. Choi, V. Va, N. Gonzalez-Prelcic, R. Daniels, C. R. Bhat, and R. W.Heath, "Millimeter-wave vehicular communication to support massiveautomotive sensing," *IEEE Commun. Mag.*, vol. 54, no. 12, pp. 160–167, Dec. 2016.
3. A. F. Molisch, M. Toeltsch, and S. Vermani, "Iterative methods forcancellation of intercarrier interference in OFDM systems," *IEEE Trans.Veh. Technol.*, vol. 56, no. 4, pp. 2158–2167, Jul. 2007.
4. G. Leus, S. Zhou, and G. B. Giannakis, "Orthogonal multiple accessover time- and frequency-selective channels," *IEEE Trans. Inf. Theory*, vol. 49, no. 8, pp. 1942–1950, Aug. 2003.



5. Z. Wang, S. Zhou, G. B. Giannakis, C. R. Berger, and J. Huang, "Frequency-domain oversampling for zero-padded OFDM in underwater acoustic communications," *IEEE Journal of Oceanic Engineering*, vol. 37, no. 1, pp. 14–24, Jan. 2012.
6. X.-G. Xia, "Precoded and vector OFDM robust to channel spectral nulls and with reduced cyclic prefix length in single transmit antenna systems," *IEEE Trans. Commun.*, vol. 49, no. 8, pp. 1363–1374, Aug. 2001.
7. T. Ebihara and G. Leus, "Doppler-resilient orthogonal signal-division multiplexing for underwater acoustic communication," *IEEE J. Oceanic Eng.*, vol. 41, no. 2, pp. 408–427, Apr. 2016.
8. R. Hadani, S. Rakib, M. Tsatsanis, A. Monk, A. J. Goldsmith, A. F. Molisch, and R. Calderbank, "Orthogonal time frequency space modulation," in *Proc. IEEE Wireless Communications and Networking Conference (IEEE WCNC'17)*, Mar. 2017, pp. 1–6.
9. A. Farhang, A. Reza zadeh Reyhani, L. E. Doyle, and B. Farhang-Boroujeny, "Low complexity modem structure for OFDM-based orthogonal time frequency space modulation," *IEEE Wireless Commun. Lett.*, vol. 7, no. 3, pp. 344–347, Jun. 2018.
10. R. Hadani, S. Rakib, S. Kons, M. Tsatsanis, A. Monk, C. Ibars, J. Delfeld, Y. Hebron, A. J. Goldsmith, A. F. Molisch, and R. Calderbank, "Orthogonal time frequency space modulation," *arXiv preprint arXiv:1808.00519*, 2018.
11. G. B. Giannakis and C. Tepedelenlioglu, "Basis expansion models and diversity techniques for blind identification and equalization of time-varying channels," *Proc. IEEE*, vol. 86, no. 10, pp. 1969–1986, Oct. 1998.
12. R. Hadani and A. Monk, "OTFS: A new generation of modulation addressing the challenges of 5G," *arXiv preprint arXiv:1802.02623*, 2018.
13. A. Monk, R. Hadani, M. Tsatsanis, and S. Rakib, "OTFS-orthogonal time frequency space," *arXiv preprint arXiv:1608.02993*, Aug. 2016.
14. M. K. Ramachandran and A. Chockalingam, "MIMO-OTFS in high doppler fading channels: Signal detection and channel estimation," *arXiv preprint arXiv:1805.02209*, 2018.
15. K. Murali and A. Chockalingam, "On OTFS modulation for high doppler fading channels," *arXiv preprint arXiv:1802.00929*, Feb. 2018.
16. W. Shen, L. Dai, J. An, P. Fan, and R. Heath, "Channel estimation for orthogonal time frequency space (OTFS) massive MIMO," *Submitted to the IEEE Trans. Signal Proc.*
17. J. Salo, G. Del Galdo, J. Salmi, P. Kysti, M. Milojevic, D. Laselva, and C. Schneider, "MATLAB implementation of the 3GPP Spatial Channel Model (3GPP TR 25.996)," Jan. 2005.  
[Online]. Available: <http://www.tkk.fi/Units/Radio/scm/>.
18. R. W. Heath, N. Gonzalez-Prelcic, S. Rangan, W. Roh, and A. Sayeed, "An overview of signal processing techniques for millimeter wave MIMO systems," *IEEE J. Sel. Top. Signal Process.*, vol. 10, no. 3, pp. 436–453, Apr. 2016.
19. X. Gao, L. Dai, S. Han, C. L. I, and X. Wang, "Reliable beamspace channel estimation for millimeter-wave massive MIMO systems with lens antenna array," *IEEE Trans. Wireless Commun.*, vol. 16, no. 9, pp. 6010–6021, Sep. 2017.
20. "Spatial channel model for multiple input multiple output (MIMO) simulations," 3GPP TR 25.996, V12.0.0 (2014-09).
21. L. Dai, B. Wang, M. Peng, and S. Chen, "Hybrid precoding-based millimeter-wave massive MIMO-NOMA with simultaneous wireless information and power transfer," *IEEE J. Sel. Areas Commun.*, vol. 37, no. 1, pp. 131–141, Jan. 2019.
22. A. Liu, V. K. N. Lau, and W. Dai, "Exploiting burst-sparsity in massive MIMO with partial channel support information," *IEEE Trans. Wireless Commun.*, vol. 15, no. 11, pp. 7820–7830, Nov. 2016.
23. D. L. Donoho, "Compressed sensing," *IEEE Trans. Inf. Theory*, vol. 52, no. 4, pp. 1289–1306, Apr. 2006.
24. L. Dai, Z. Wang, and Z. Yang, "Spectrally efficient time-frequency training OFDM for mobile large-scale MIMO systems," *IEEE J. Sel. Areas Commun.*, vol. 31, no. 2, pp. 251–263, Feb. 2013.